



Impact of wear parameters on NiCr-WC10Co4Cr and WC10Co4Cr HVOF sprayed composite coatings using response surface methodology

Azzeddine Mazouzi¹ · Amine Rezzoug² · Billel Cheniti² · Seif El Islam Lebouachera³ · Djamel Miroud¹ · Aniss-Rabah Boukantar¹ · Nadjib Drouiche⁴ · Boubekeur Djerdjare¹

Received: 24 December 2020 / Accepted: 8 March 2021 / Published online: 17 March 2021
© The Author(s), under exclusive licence to Springer-Verlag London Ltd., part of Springer Nature 2021

Abstract

In the present paper, experimental and statistical studies of wear behavior of two HVOF sprayed coatings (NiCr-WC10Co4Cr (Coat1) and WC10Co4Cr (Coat2)) deposited on 304L austenitic stainless steel have been investigated. Applied load, sliding velocity, and distance are the most important parameters that directly affect the wear volume of a given coating. In order to quantify the influence of each parameter on the wear rate of both coatings, two different loads (5 and 15 N), velocities (5 and 20 cm/s), and distances (500 and 1500 m) are selected to perform the experimental study. The microstructural study conducted on both coatings using scanning electron microscopy (SEM) and X-ray diffraction (XRD) technique reveals a dissolution of WC particles into the NiCr matrix with the formation of W_2C eutectic phase that affects the coatings during tribology tests. The wear mechanism appears to be abrasive for Coat2 and combined mechanism of adhesive and abrasive wears in the case of Coat1. Based on the mathematical model developed using response surface methodology (RSM), the results show that both coatings yield the same response in terms of RSM individual output. In addition, RSM reveals that the normal load is the most significant individual parameter affecting wear volume with *t*-ratio of 46.11 and 32.00 of Coat1 and Coat2, respectively. However, the interaction of parameters is different regarding the nature of the coating. Normal load-sliding velocity interaction is the most influencing in Coat1, while Coat2 wear behavior is more influenced by sliding distance-normal load interaction.

Keywords NiCr · WC10Co4Cr · HVOF composite coating · Wear volume · Tribological behavior · RSM

1 Introduction

Improving the surface properties by developing a coating of high density, high bond strength, high hardness, and refined microstructure is the prime requirement of surface engineering

✉ Amine Rezzoug
a.rezzoug@crti.dz

¹ Science and Engineering Materials Laboratory (LSGM), USTHB, BP 32 El Alia, 16111 Bab Ezzouar, Algeria

² Research Center in Industrial Technologies (CRTI), P.O. Box 64, Cheraga, 16014 Algiers, Algeria

³ Institut des Sciences Analytiques et de Physico-chimie pour l'Environnement et les Matériaux, IPREM, UMR 5254, CNRS Université de Pau et des Pays de l'Adour/E2S, 2 avenue P. Angot, Technopôle Hélioparc, 64000 Pau, France

⁴ CRTSE-Division CCPM- N°2, Bd Dr. Frantz FANON, P.O.Box 140, 16038 Alger sept merveilles, Algeria

for enhanced performance against wear [1]. From an economical perspective, wear is considered as a critical problem in industries, which limits the good behavior and lifetime of materials' surface in tribological point of view [2, 3]. Abrasive and adhesive wears cause the failure of engineering components that are subjected to friction in the industry [1, 4]. Therefore, surface modification is required to increase the life span of mechanical parts used in severe working conditions [5]. Among the techniques used to enhance the surface characteristics is coating. Thermal spray is an effective method for surface characteristic modification of engineering compounds widely used in several industrial applications where high-velocity oxy fuel (HVOF) spray technique of hard materials coating is the most technique used in aeronautic, sand pumps, and tool bit coating [6]. In fact, a low porosity level and very high adhesion strength of various cermets and composite materials such as: WC-Co, NiCr and Cr_3C_2 are guaranteed by HVOF technique compared to other coating processes [7, 8]. NiCr-based alloy is generally used as a binder with hard particles; it provides good

resistance against corrosion and oxidation of the coating with high wettability level for the cermet (adhesion improvement) [9, 10]. Considerable attention has been paid to WC-Co-Cr composite HVOF spraying due to the well-adhered and dense coating, which combine good stiffness of WC and high toughness of Co and Cr elements. In fact, wear resistance of WC particles with high hardness combined with the tough and ductile CoCr matrix enable the wide application of the composite in severe working conditions [11, 12].

The interaction between the various parameters during wear tests raises much difficulty to understand the effect of individual parameters on the wear behavior of the studied material. Hence, modeling exhibited for a long time the potential to solve complicated problems, with reduced test number and optimized the results [13]. Response surface methodology (RSM) has become an effective statistic method widely employed to solve engineering problems and the interpretation of the technical result. The input variables influence some performance over the output variables. RSM provides quantitative measurements of possible interactions between parameters, which are difficult to obtain using other techniques of optimization [14, 15]. Several research works have investigated the application of RSM to optimize the characteristics of a given process. This method reduces remarkably the number of trials required to respond to the model [16–19]. Therefore, many previous works highlighted the impact of wear parameters of the coating behavior using this method. Sail et al. [20] investigated the effects of sliding velocity, sliding distance, and normal load on output responses (dynamic friction coefficient, wear volume, and total roughness) by sliding wear test onto (Ti-W-N) coating using pin-on-disk machine. They found that the dynamic coefficient of friction decreases linearly with the increase in normal load basing on RSM. In addition, there is a proportional increase in the wear volume as the sliding distance increases, whereas a slight increase can be seen when the normal load is increased. According to Sharma et al. [21], the load and sliding distance have severe effect on abrasive wear of the coating as compared to abrasive size of Ni-WC-CeO₂ composite HVOF sprayed coatings. On the other side, Saravanan et al. [18] optimized wear behavior of biocompatible TiN material coated on 316L SS against Ti alloy using RMS. They concluded that the minimal specific wear rate and coefficient of friction were obtained when adjusting the optimal input parameters of sliding. Hence, this method shows the potential to be a procedure that deals with the responses influenced by multi-variables such as wear parameters. There is limited information dealing with using RSM to study the tribological behavior of WC-based hard coatings. This work aims to figure out the individual and combined impacts of wear parameters (load, distance, and velocity) on the wear volume of two different coatings (NiCr-WC10Co4Cr (Coat1) and WC10Co4Cr (Coat2)) deposited on 304L stainless steel using HVOF process. In addition, the optimal

conditions at which the wear volume is the lowest are determined, based on desirability function method developed by Derringer and Suich [22], which is widely used to solve problems linked to the optimization of multiple responses related to the industry. Experimental and statistical investigations of the tribological behavior of the coatings is conducted. RSM modeling technique is used to estimate the effect of the experimental parameters on the tribological performance (friction coefficient and wear mechanisms) of both coatings.

2 Materials and experimental procedures

The substrate considered in this work is 304L austenitic stainless steel (304L SS), widely used in various aggressive environments because of its excellent corrosion resistance. However, the tribological proprieties of this material need to be improved when it is used in severe wear conditions, such as downhole tools. The nominal composition for substrate is (wt.%) C 0.03%, Si 1.00%, Mn 2.00%, P 0.045%, S 0.03%, Cr 19.5%, Ni 10%, and Fe (balance) (Deperly Dufour, France). NiCr and WC10Co4Cr powders are achieved by an atomization process and have a particle size ranging from about 15 to 45 μm (Wisdom Company, Shanghai, China). The SEM analysis of these powders is shown in Fig. 1. The shape of both powders is nearly spherical with a certain degree of porosity regarding WC10Co4Cr powder. The nominal chemical composition (wt.%) was obtained by EDS analysis. From Fig. 1a, NiCr powder presents 76.96% of Ni and 23.04% of Cr. From Fig. 1b, WC10Co4Cr powder presents 89.88% of W, 7.35% of Co, and 2.78% of Cr. Using the HVOF process; the selected parameters for spraying operation are presented in Table 1. The powders are sprayed using an HJ2700 gun (Metalizing Equipment Corporation LTD, Rajasthan, India). Disks of 25-mm diameter and 5-mm thickness (304L SS) were coated by two coatings: NiCr-WC10Co4Cr (Coat1) and WC10Co4Cr (Coat2) with a thickness of about 300 μm .

The microstructures of the powders, the coatings, and worn surfaces were examined by SEM (JEOL, JSM6830, Japan) equipped with an energy-dispersive spectroscopy (EDS) apparatus. XRD analyses were performed using a Philips diffractometer, with 40 kV, a Cu ($K\alpha$) = 0.15406 nm, and a step size 0.05°/s. The recorded XRD patterns are characterized by PANalytical X'Pert High Score software; the average phase fractions were determined by XRD data sets for each sample.

In order to determine the mechanical properties of coatings' phases, nano-indentation measurements were carried out. Using Nanoindenter (Anton Paar NHT-3) with Berkovich tip under 100-mN applied load, the test was conducted onto the matrix and reinforcements (carbide). The final values of hardness and Young's modulus were obtained for an average value of 3 tests.

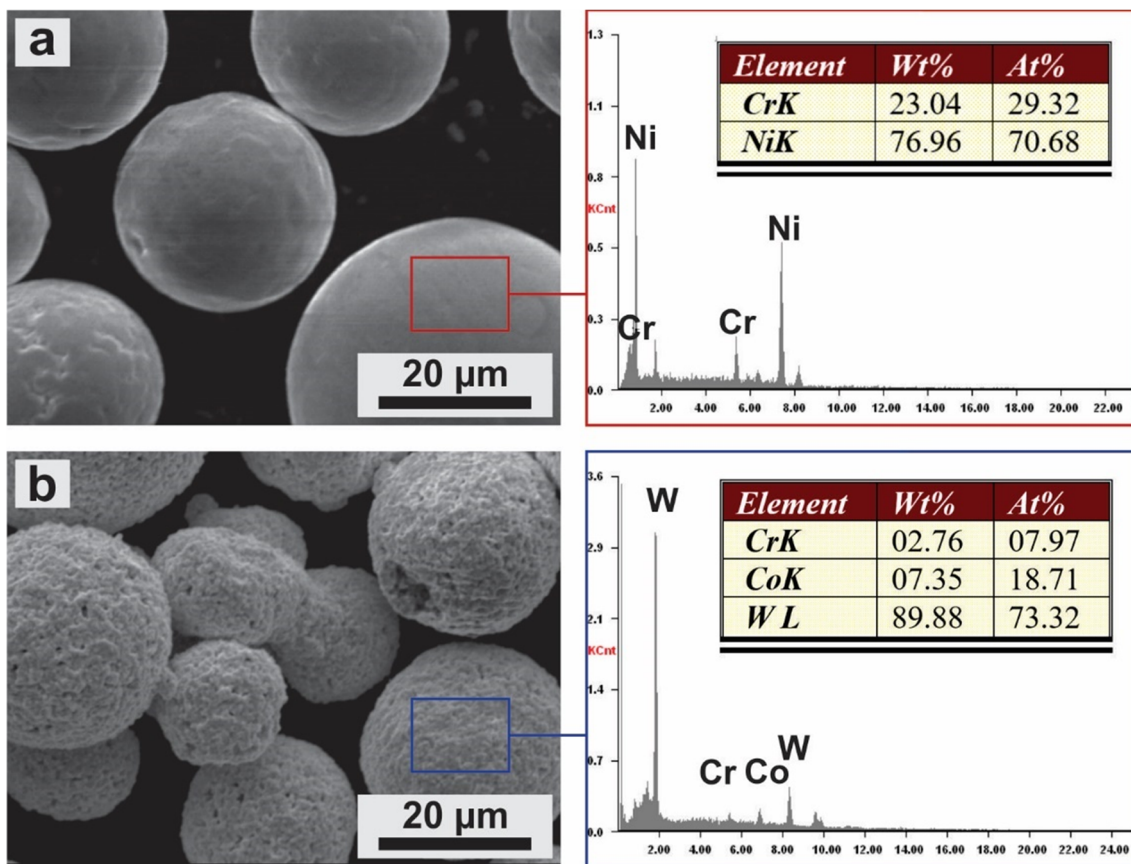


Fig. 1 SEM images and EDS analysis of powders. a NiCr and b WC10Co4Cr

Tribological tests were carried out on a ball-on-disk tribometer (CSM tribometer, CSM instruments inc, Peseux, Switzerland), according to ASTM G99-0516. The disk was initially cleaned with acetone. The tests were carried out by applying normal loads of 5 and 15 N and run for two sliding distances of 500 and 1500 m at two different sliding velocities of 5 and 20 cm/s. The level’s factors of testing methodology are presented in Table 2. An Al₂O₃ ball of 6 mm is placed in contact with the sample surface. All tests were conducted at room temperature under dry laboratory conditions, by considering 10 mm as tribological diameter. During sliding, the friction coefficient (CoF) was continuously measured and recorded in real time by the computer software of the tribometer

(TriboX). The width of the wear track (d) was determined via micrographs using optical microscopy (Eclipse 3000, Nikon Instruments, Melville, NY, USA) and image analysis software (ImageJ). At least four measurements were taken per sample at different positions over the wear track, and the average values were reported. At the end of each test, the wear volume (W) in mm³ of each specimen is calculated using Eq. (1).

$$W = 2\pi R \left[r^2 \sin^{-1}(d/2r) - (d/4)(4r^2 - d^2)^{(1/2)} \right] \tag{1}$$

where R is the radius of the wear track (mm), d is the width of the wear track (mm), and r is the radius of the ball (mm).

Table 1 Spray parameters using HJ2700 gun

Gun	HJ2700
Fuel	LPG
Spray distance	180 mm
Oxygen flow rate	500–600 L/min
Powder feed	25–38 gm/min
Deposition efficiency	60–70%
Traverse rate	0.0028–0.0030 m/s

Table 2 Factors and levels used in the factorial design 2³

Codes	Control factors	Low level -1	High level +1
X ₁	Sliding distance (m)	500	1500
X ₂	Normal load (N)	5	15
X ₃	Sliding velocity (cm/s)	5	20

In this work, a full 2^3 factorial design that requires eight experiments is used to study the importance of the individual effects and the interactions of test parameters on the wear volume. The chosen design helps to reduce the number of experiments and the time to reach the appropriate model for the optimization process. The 2^k represents the number of experiments, and k is the number of factors. Three input variables such as sliding distance (m) “ X_1 ,” normal Load (N) “ X_2 ,” and sliding velocity (cm/s) “ X_3 ” have been varied. Hence, one response is evaluated as an experimental wear volume (mm^3) and is denoted as “ Y_1 ” and “ Y_2 ” for NiCr-WC10Co4Cr and WC10Co4Cr coating, respectively.

The results of the factorial design were studied and interpreted statistically based on analysis of variance (ANOVA), and the determination of coefficient R^2 was calculated using the JMP 13 software. The significance of the regression coefficient parameters is discussed by Student’s t -test. The choice of distance (m) “ X_1 ,” normal Load (N) “ X_2 ,” and sliding velocity (cm/s) “ X_3 ” is among the most important parameters that affect the wear volume [20]. The higher level is designated by +1 and the lower level by –1, which appears in Table 2 for the parameters studied. Hence, the design matrix of coded values for different

factors which are codified with mathematical model for the 2^3 is given as:

$$Y = a_0 + a_1X_1 + a_2X_2 + a_3X_3 + a_{12}X_1X_2 + a_{13}X_1X_3 + a_{23}X_2X_3 \quad (2)$$

The response Y is considered as the experimental wear volume (mm^3). The run order of experiments is carried out from the right to the left to correct the possible experimental errors based on the Yates’ algorithm and applied in the case of all 2^k factorial experiments [23, 24].

In as much as Y represents the experimental wear volume (mm^3), the constants a_0 , a_i , and a_{ij} represent the global mean. The regression coefficients are assigned respectively to the principal factor effects and interactions.

3 Results and discussion

3.1 Surface coating and tribological behavior

Figure 2a and b show the cross-sectional microstructure of NiCr-WCCoCr (Coat1) and WCCoCr (Coat2) coatings,

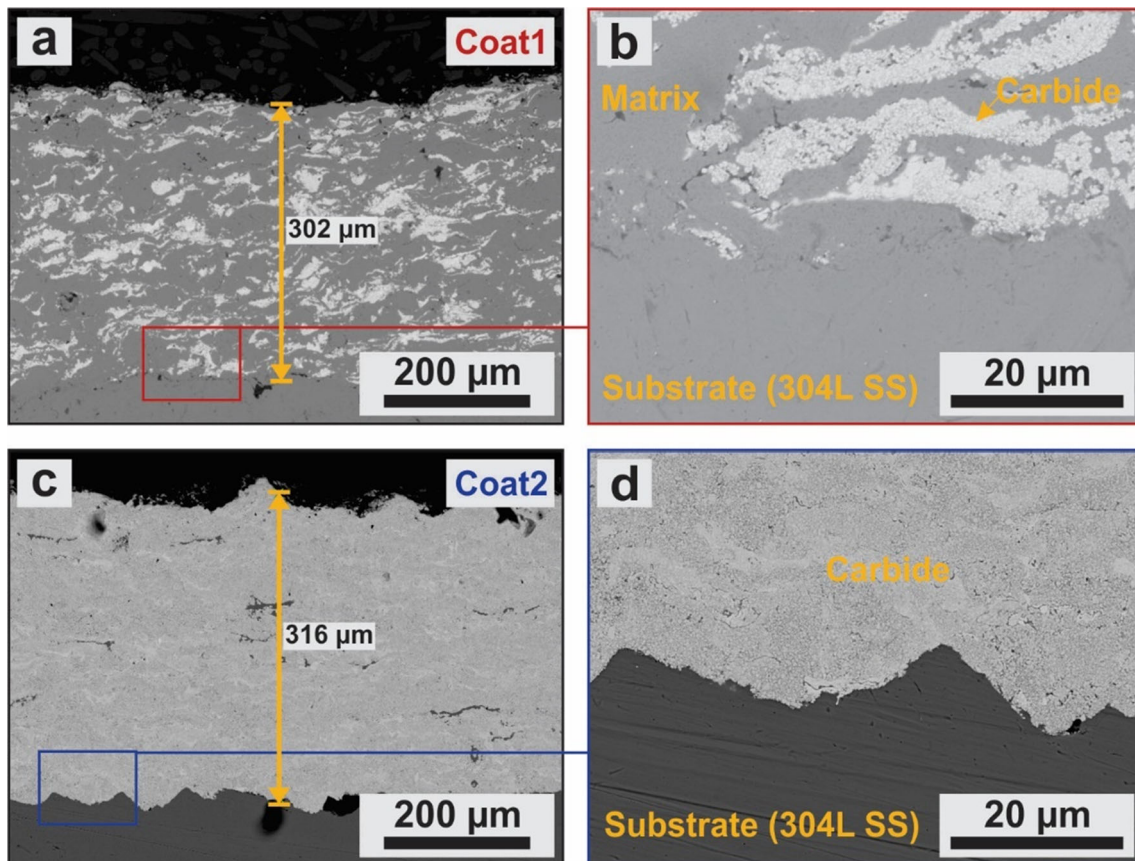


Fig. 2 SEM cross-sectional microstructure of a, b Coat1 (NiCr-WC10Co4Cr) and c, d Coat2 (WC10Co4Cr)

respectively. Both coatings exhibit a thickness of about 300 μm with no cracks or delamination defects with a good adhesion aspect of coatings/substrate interfaces as shown in Fig. 2c and d. It is seen that particles in Coat1 and Coat2 are partially melted where Coat2 shows higher interparticle porosity level compared to Coat1, which are in good agreement with the findings in previous research works [25, 26]. XRD patterns of the feedstock powders and the as-sprayed coatings (Coat1 and Coat2) are shown in Fig. 3a, b, c, and d). The XRD results of the powders (Fig. 3a and b) show that NiCr and WC are the most prominent phases, while Ni and Co exhibit small peaks indicating their small content. The as-sprayed coatings reveal the presence of a new W_2C phase in both coatings (Fig. 3c and d) with a broad peak observed between 40 and 50° in Coat2 (Fig. 3d) that may be related to the differential dissolution of the WC carbide in the NiCr matrix and to the presence of partially amorphous/fine crystalline phases [27]. On the other side, it can be seen that, after HVOF spraying, the peaks of WC and NiCr phases shift due to residual stresses induced by the plastic deformation of the particles during their interaction with the substrate surface at high temperature. Furthermore, it can be observed the disappearance of Co peak in Coat2, which is probably attributed to the dissolution of W element into the Co-Cr matrix and the formation of W-Cr-Co

amorphous phase after rapid solidification [28, 29]. In addition, the decarburization degree of WC particles and the formation of W_2C eutectic phase are lower in Coat2 compared to that in Coat1. This phenomenon can be explained by the high chemical affinity between Cr and C elements that accelerates the WC particle dissolution in Coat1 due to the presence of high amount of Cr element in the matrix. Similar results were reported in the previous works [7, 28, 29] when HVOF spray is used to deposit such materials.

Figure 4 shows SEM micrograph of the as sprayed Coat1 with the corresponding EDS mapping analysis. It is seen that the WC particles change their original spherical shape and transform into splat-like structure due to the plastic deformation generated during the impact of the particles on the steel substrate surface at high temperature and velocity. The EDS mapping analysis reveals the heterogeneous distribution of C element throughout the coating; it is accentuated where W and Cr elements were located. This confirms the presence of WC, CrC carbides, and more probably W_2C eutectic carbide already found by XRD experiments. On the other side, homogeneous distribution of Ni and Cr elements is observed through the Coat1-substrate interface, which may reflect the good metallurgical bonding of the coating. The interaction between WC particles and the steel substrate in Coat2 with

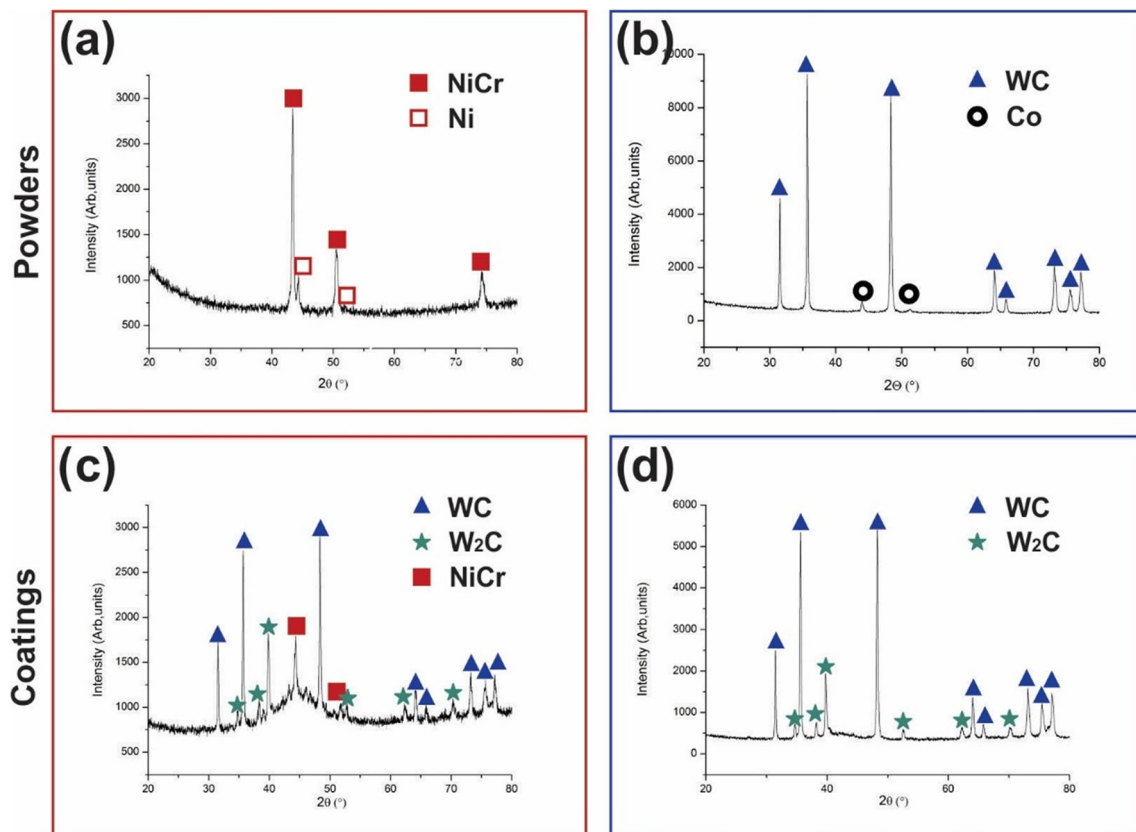


Fig. 3 XRD patterns of feedstock powder and sprayed coating. **a** NiCr and **b** WC10Co4Cr powders, respectively. **c** Coat1 (NiCr-WC10Co4Cr) and **d** Coat2 (WC10Co4Cr), respectively

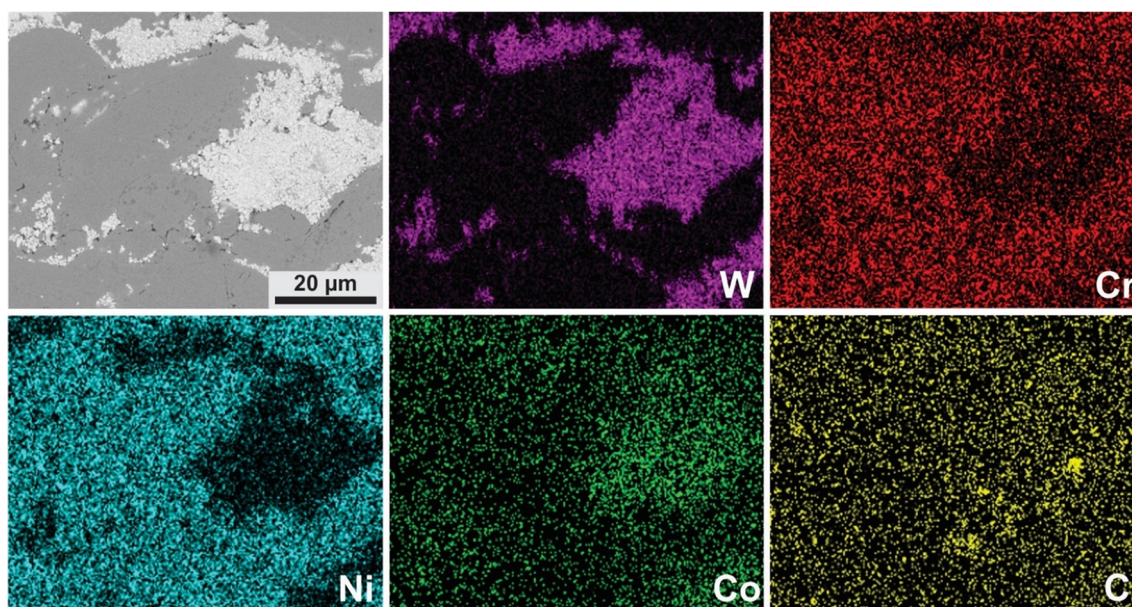


Fig. 4 SEM mapping at the cross section of Coat1 (NiCr-WC10Co4Cr)

the EDS mapping analysis is illustrated in Fig. 5. It can be seen that no inter-diffusion of elements along the Coat2-substrate interface is allowed when WC particles are at the vicinity of the substrate. The WC-steel contact results in poor metallurgical bonding and weakens the interface by inhibiting the element diffusion activity throughout the interface, which may have a direct effect on the coating properties. On the other side, the EDS point analysis conducted in Coat1 (Fig. 6 and Table 3) reveals that the concentration of W element (spot D) decreases from the middle of WC particle, to 83 wt. % (spot B), to the interface with the NiCr matrix (spot A), suggesting that the dissolution of WC particles into the matrix due to the solubility of W in Ni (~ 9%), in agreement with the W-Ni binary phase diagram. The low-contrast zones present in the carbide (C and E) contain significant amount of Ni; that could

be attributed to the new eutectic phases such as W_2C and W_4Ni [30].

Nano-indentation measurements conducted in the matrix and carbide of Coat1 (NiCr-WC10Co4Cr) are shown in Fig. 7a. As expected, the penetration depth in the load-displacement curves was found to be greater on the matrix compared with the carbide. Furthermore, the slope of the unloading segment of the carbide appears to be steeper than of measured for the metallic matrix. The corresponding hardness (H_{IT}) and elastic modulus (E_{IT}) values for each of the tested zones were calculated using the Oliver and Pharr method [31] and are summarized in Fig. 7b. As a result of the presence of hard WC particles, the measured hardness in this zone is obviously higher (~ 32 GPa) than the matrix zone which is mainly composed of NiCr

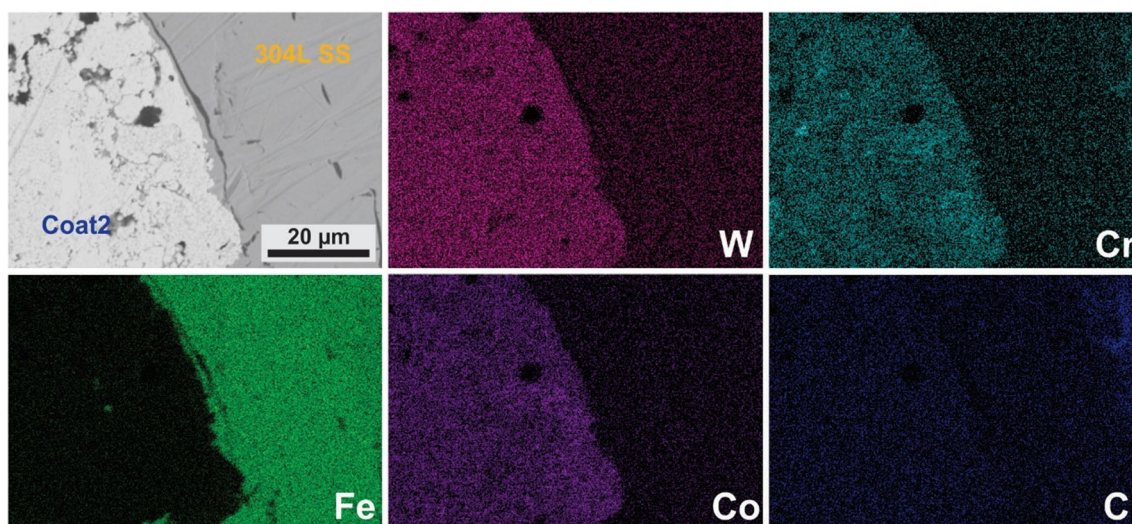


Fig. 5 SEM mapping at the cross section of Coat2 (WC10Co4Cr)

Fig. 6 SEM micrographic and EDS analysis of Coat1 (NiCr-WC10Co4Cr) in different zones

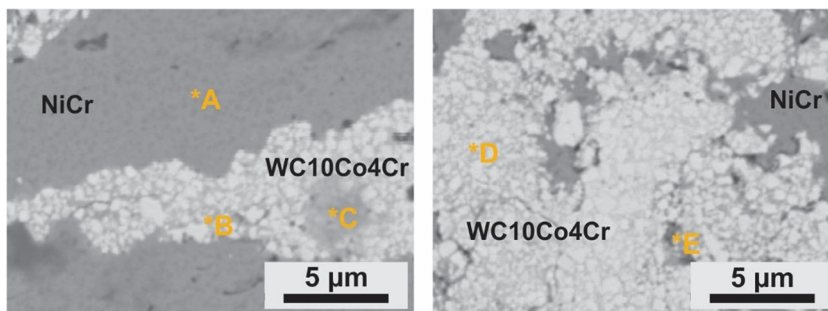


Table 3 EDS analyses conducted at the cross section of Coat1 in Fig. 6

Element (Wt.%)	W	Ni	Cr	Co	Fe	C
A	/	74.18	21.84	/	3.78	/
B	83.27	/	5.94	10.79	/	/
C	28.83	12.19	20.00	8.77	/	30.21
D	91.18	/	/	8.82	/	/
E	72.06	11.43	6.07	08.68	1.75	/

(ductile phase). Meanwhile, the Young’s modulus of the carbide (about 525 GPa) was also higher than that of the matrix (about 190 GPa), which may affect the tribological behavior of the studied coatings.

The evolution of friction coefficients (CoF) of the coatings for various parameters is presented in Fig. 8a, b, c, d, and e. It can be seen that roughly all the curves exhibit two stages of friction: (i) the first stage is characterized by initial run-in period with rapid increase followed by a decrease of CoF, and (ii) the second one is the steady-state stage where the CoF slightly increases and stabilizes at a constant value. It is

assumed that the increase of CoF during the first stage is strongly related to the surface coating roughness accommodated with the Al_2O_3 ball counterpart. Nevertheless, the formation of the third body promotes the stabilization of the CoF after a running distance that is related to load and sliding velocity [30]. The results show that, whatever the test parameters (distance, applied load, and velocity), the CoF of Coat1 are higher than the Coat2 ones (Fig. 8e), while the CoF increase with rise in sliding velocity and load. In fact, the plastic deformation induced by the Al_2O_3 counterpart during sliding strengthens the coating’s surface by hardening the ductile NiCr matrix (low hardness and elastic modulus), which allows the increase of CoF in Coat1. In contrast, the large amount of WC hard particles (high hardness and Young’s modulus) act as lubricious oxide tribolayer in Coat1 [32, 33]. This result correlates with the results of A.C. Karaoglanli et al. [11] when comparing the tribological behavior of hard coating with the relative soft ones. With increasing sliding distance, more debris are generated as a result of the plastic deformation of the worn surfaces subjected to a constant load. Simultaneously, important abrasive particle fragmentation occurs with an increase in applied load. On the other side, increasing velocity generates the removal of tribo-oxide film by delamination

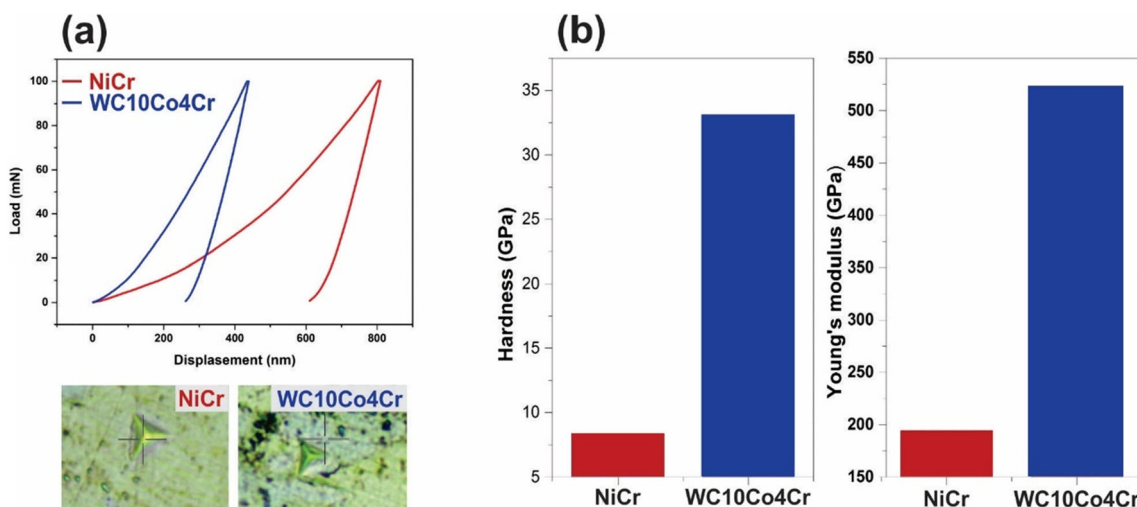


Fig. 7 Nano indentation measurement at the matrix (NiCr) and the carbide (WC10Co4Cr) of Coat1. **a** Load displacement curves at 100 mN. **b** Hardness and Young’s modulus

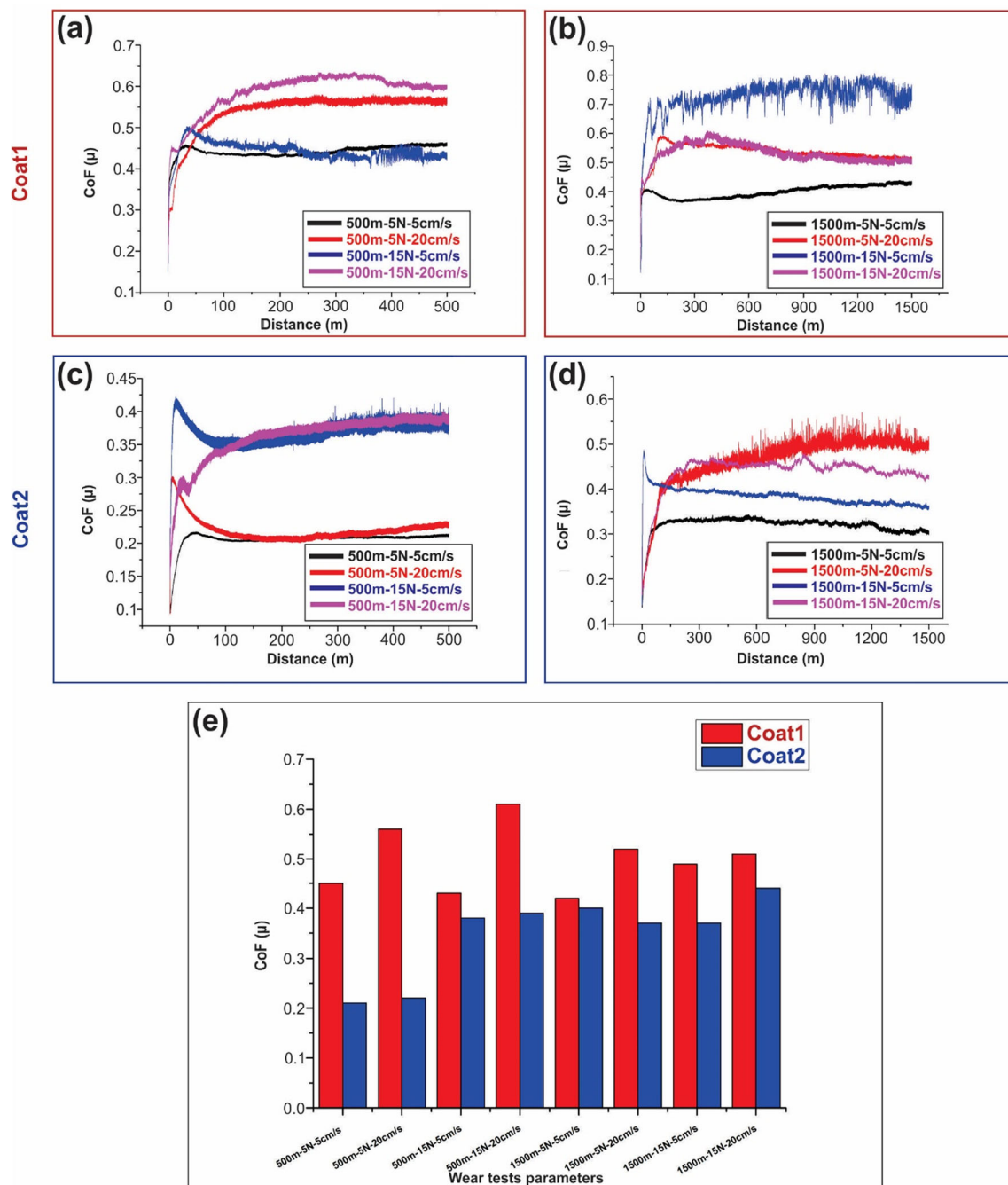


Fig. 8 Evolution of friction coefficient as a function of sliding distance. **a** and **b** Coat1 (NiCr-WC10Co4Cr) at sliding distance of 500 and 150 m, respectively. **c** and **d** Coat2 (WC10Co4Cr) at sliding distance of 500 and

150 m, respectively. **e** Variation of friction coefficient according to parameters and coatings

cracking and more probably fracture of the surface, which results in oxide debris formation that increases the CoF with increasing velocity particularly at higher loads.

SEM micrographs of worn surfaces for both coatings after the extreme wear conditions (15N load, 1500 m sliding distance, and 20 cm/s velocity) are shown in Fig. 9a, b, c, d, and e. The wear track on Coat1 (Fig. 9a) exhibits a smoother aspect compared to that on Coat2 (Fig. 9d) with grooves parallel to the sliding direction. The cutting process responsible

for the grooves is related to the presence of hard particles (WC) detached from the WC10Co4Cr and trapped on Coat1 [34], while the low hardness of NiCr matrix compared to Al₂O₃ counterpart resulted in the plastic deformation of the coating surface (Coat1) for short sliding distance. Nevertheless, after long sliding distance, plastic shear deformation is occurred resulting in adhesive wear mechanism as seen in Fig. 9b and c. These observations suggest the presence of a combined mechanism of adhesive and abrasive wears in

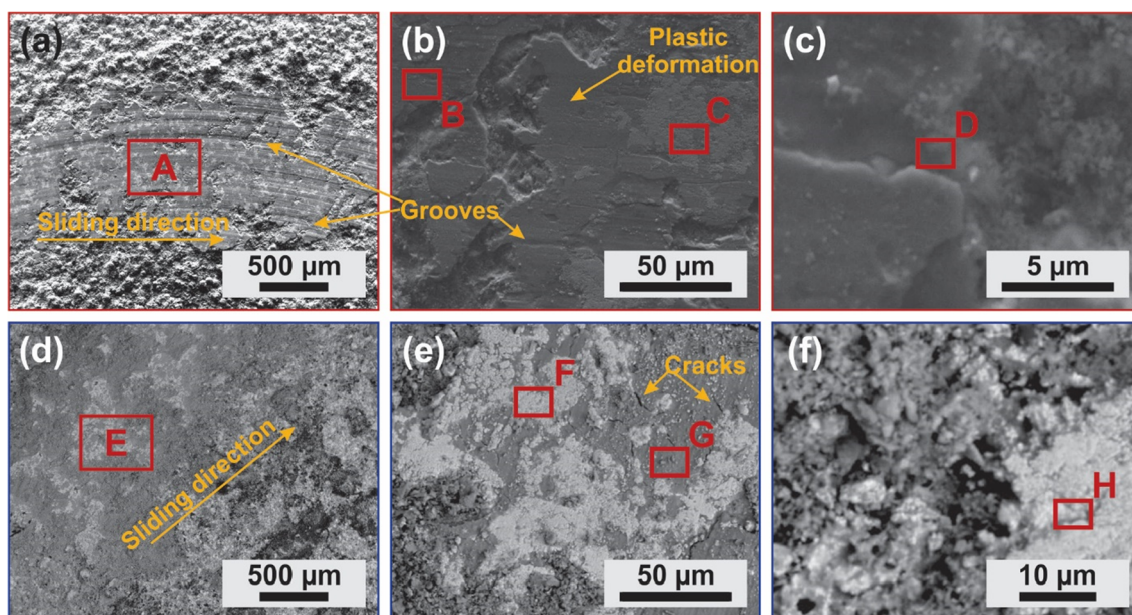


Fig. 9. SEM of worn surface after wear test at sliding distance of 1500 m, normal load of 15 N, and sliding velocity of 20 cm/s. **a, b, c** Coat1. **e, f** Coat2

the case of Coat1 [35]. On the other hand, the rougher morphology of Coat2 wear track (Fig. 9d) indicates that brittle fracture occurred during sliding with some cracks (Fig. 9e) resulting from the abrasive wear mechanism. This phenomenon is more likely attributed to the decohesion and the pull out of the WC particles due to the formation of W_2C hard eutectic phase [36]. With the remarkably high hardness of WC10Co4Cr compared with that of NiCr matrix (see Fig. 7b), more abrasive wear in Coat2 is observed. The EDS analyses carried out on different zones of the worn surface summarized in Table 4 reveal the presence of 5.38 wt.% of Al (spot B with respect to A) in Coat1 detached from the counterpart ball and adhered to the ductile surface of NiCr matrix. The presence of W in the surface of NiCr matrix (point B) and Ni in the surface of WC10Co4Cr particles (spots C and D) suggests that hard debris adheres on ductile surface and vice versa. On the other hand, the significant presence of oxygen (spot G compared to spot H) on the Coat2 surface may be explained by the formation of WO_3

[37]. Note that the presence of Al element (spots E and F) on the coatings' worn surfaces suggests more probably the abrasive wear of the Al_2O_3 ball counterpart.

3.2 Factorial design of experiments

In order to better understand the effect of the test conditions on the tribological behavior of the studied coatings, load, distance, and velocity are chosen as wear parameters. Several sliding wear tests were conducted with various parameters (Table 5) to estimate their impact on the wear volume of Coat1 and Coat2 based on RSM. The tribological behavior is calculated in terms of the wear volume (mm^3) for Coat1 and Coat2 with respect to independent factors (sliding distance, normal load, and sliding velocity considering two parameters level -1 and $+1$ as low and high values of each parameter (full factorial L8), respectively.

The RSM trials of the randomized design values are shown in Table 5. The optimization is based on the “smaller the best” concept, so that the parameters with low wear volume are considered as optimum. From this concept, it can be seen that the wear volume is obtained in the range from 0.213 to 1.020 mm^3 regarding Coat1 and from 0.170 to 0.870 mm^3 for Coat2. The low wear volumes of Coat2 are attributed to the higher hardness of the coating due to the presence of WC hard particles that lowers the CoF compared to that of Coat1 as discussed in Sect. 3.1. From Table 6, and based on Student's t -test of Coat1 that confirms the validity of regression coefficients, it is clear that when t -value is higher than t -critic (t -critic equals 0.15), the regression and the coefficient are statistically significant [38]. Also, for reliability consideration, R^2 that equals to 0.99 indicates that the model is in good

Table 4 EDS analyses for worn surface of Coat1 (NiCr-WC10Co4Cr) and Coat2 (WC10Co4Cr) coatings at points shown in Fig. 9

Element (Wt.%)	W	Ni	Cr	Co	Al	O	Fe	C
Coat1	A	38.35	45.44	11.82	1.75	/	/	2.64
	B	46.25	34.06	9.89	2.31	5.38	/	2.11
	C	70.73	13.21	6.47	7.03	0.13	2.43	/
	D	84.08	4.12	3.94	7.86	/	/	/
Coat2	E	63.24	/	3.03	7.58	5.91	15.62	4.62
	F	81.94	/	3.14	9.36	0.78	5.17	/
	G	58.53	/	/	9.27	0.44	28.48	/
	H	85.81	/	3.85	10.81	/	/	/

Table 5 Experimental design using full factorial L8 orthogonal array for each coating

Samples	Coded factors			Actual factors			Response Item Wear volume W (mm ³)	
	X ₁	X ₂	X ₃	D(m)	P(N)	V(cm/s)	Coat1	Coat2
1	-1	-1	-1	500	5	5	0.213	0.170
2	-1	-1	+1	500	5	20	0.397	0.360
3	-1	+1	-1	500	15	5	0.525	0.489
4	-1	+1	+1	500	15	20	0.954	0.620
5	+1	-1	-1	1500	5	5	0.275	0.190
6	+1	-1	+1	1500	5	20	0.525	0.445
7	+1	+1	-1	1500	15	5	0.437	0.722
8	+1	+1	+1	1500	15	20	1.020	0.870

agreement with the response [39]. By substituting in Eq. (2) the regression coefficient values as shown in Table 6, we get:

$$W_1 \text{ (mm}^3\text{)} = 0.5495 + 0.02725*X_1 + 0.219*X_2 \\ + 0.1525*X_3 + 0.00175*X_1*X_2 \\ + 0.00075*X_1*X_3 + 0.066*X_2*X_3.$$

All coefficient values have positive sign in the polynomial model; this indicates their positive influences on the wear volume response.

It can be noted from the obtained data that the normal load (X₂) is the most important parameter for the overall wear volume process with a high *t*-ratio equals to 46.11; hence, it can be said that the normal load exerts a strong influence on the wear volume. Subsequently, the sliding velocity is the second more influencing parameter with a *t*-ratio of 32.11,

while sliding distance is found to be the least significant parameter with a *t*-ratio of 5.57. Interaction between X₂ and X₃ at a high *t*-ratio of 13.89 is the most significant combination compared to (X₁, X₃) and (X₁, X₂) with a *t*-ratio of 0.16 and 0.37, respectively. It also appears that the normal load, sliding distance, and sliding velocity have a direct effect on the wear behavior. The same trend was observed for the interaction effects between sliding distance and normal load. This result confirms that the model is highly significant with the *p* value of 0.0322 less than 0.05 [22] and the *F*-ratio of 563.7632, cited below in the ANOVA analysis.

By substituting regression coefficients in Eq. (2), as given in Table 7, we get:

$$W_2 \text{ (mm}^3\text{)} = 0.48325 + 0.0735*X_1 + 0.192*X_2 \\ + 0.0905*X_3 + 0.04725*X_1*X_2 \\ + 0.01025*X_1*X_3 - 0.02075*X_2*X_3.$$

Table 6 ANOVA response for wear volume model of Coat1 (NiCr-WC10Co4Cr)

Source	Estimate	Standard error	<i>t</i> -ratio	<i>p</i> value
Intercept	0.5495	0.00	115.68	0.0055*
X ₁ : sliding distance	0.02725	0.00475	5.57	0.1099
X ₂ : normal load	0.219	0.00475	46.11	0.0138*
X ₃ : sliding velocity	0.1525	0.00475	32.11	0.0198*
X ₁ × X ₂	0.00172	0.00475	0.37	0.7753
X ₂ × X ₃	0.00075	0.00475	0.16	0.9003
X ₂ × X ₃	0.066	0.00475	13.89	0.457*
<i>R</i> ² = 0.999704				
<i>R</i> ² adjusted = 0.997931				
Root mean square error = 0.013435				
Mean of response = 0.5495				
Analysis of variance (ANOVA)				
Source	DF	Sum of square	Mean square	<i>F</i> -ratio 563.7632
Model	6	0.61055550	0.101759	Prob 0.0322
Error	1	0.00018050	0.000181	
C.Total	7	0.6173600	/	
* <i>p</i> <0.05				

Table 7 ANOVA response for wear volume of Coat2 (WC10Co4Cr)

Source	Estimate	Standard error	<i>t</i> -ratio	<i>p</i> value
Intercept	0.48325	0.006	80.54	0.0079*
X ₁ : sliding distance	0.0735	0.006	12.25	0.0519
X ₂ : normal load	0.192	0.006	32.00	0.0199*
X ₃ : sliding velocity	0.0905	0.006	15.08	0.0421*
X ₁ × X ₂	0.04725	0.006	7.87	0.0804
X ₁ × X ₃	0.01025	0.006	1.71	0.3371
X ₂ × X ₃	-0.02075	0.006	-3.46	0.1792
<i>R</i> ² = 0.999324				
<i>R</i> ² adjusted = 0.995269				
Root mean square error = 0.016971				
Mean of response = 0.48325				
Analysis of variance				
Source	DF	Sum of square	Mean square	<i>F</i> -ratio
Model	6	0.42579750	0.070966	246.4106
Error	1	0.00028800	0.000288	Prob 0.0487*
C.Total	7	0.42608550	/	

**p*<0.05

From the above expression, the values of the coefficients have a positive sign, indicating their positive influences on wear volume response, except the last constant that has a negative value.

From Table 7, it can be stated that similarly to Coat1, the normal load (X₂) is the most important parameter for the overall wear volume process for Coat2 with high *t*-ratio of 32.00, suggesting that the normal load exerts a strong influence on the wear behavior. Velocity is considered to be the second important parameter followed by sliding distance. Contrary to Coat1, in Coat2, the interaction of X₁ and X₂ with a high *t*-ratio of 7.87 is the most significant than all other combinations, while the combination (X₂ and X₃) is reflected to be the least significant parameter with a *t*-ratio of -3.46. The wear behavior of Coat1

which contains ductile matrix (NiCr) is greatly influenced by sliding velocity when combined with normal load; this is because of the plastic deformation which makes the sliding of the ball difficult at high velocity. On the other hand, since hard coating (Coat2) does not present ductile deformation, the matter is loosed progressively with the increase of the duration of the test (sliding distance) by abrasive wear.

For Coat2, ANOVA result shows also the existence of linear effects on the normal load, sliding distance, and sliding velocity. The same trend is observed for the interaction effects between sliding distance and normal load, which confirms that the model is also highly significant with both *p* value of 0.0487 less than 0.05 [22] and *F*-value of 246.4106 cited in ANOVA analysis below.

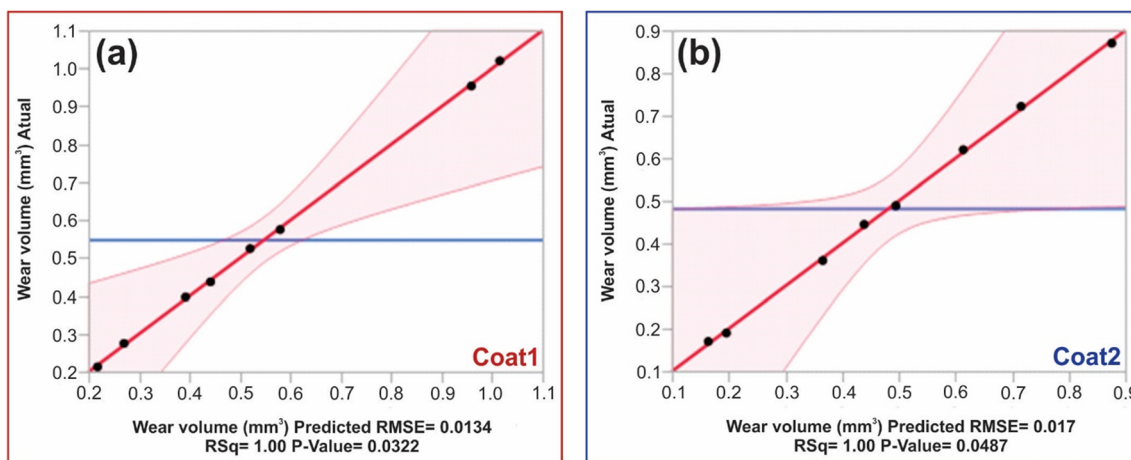
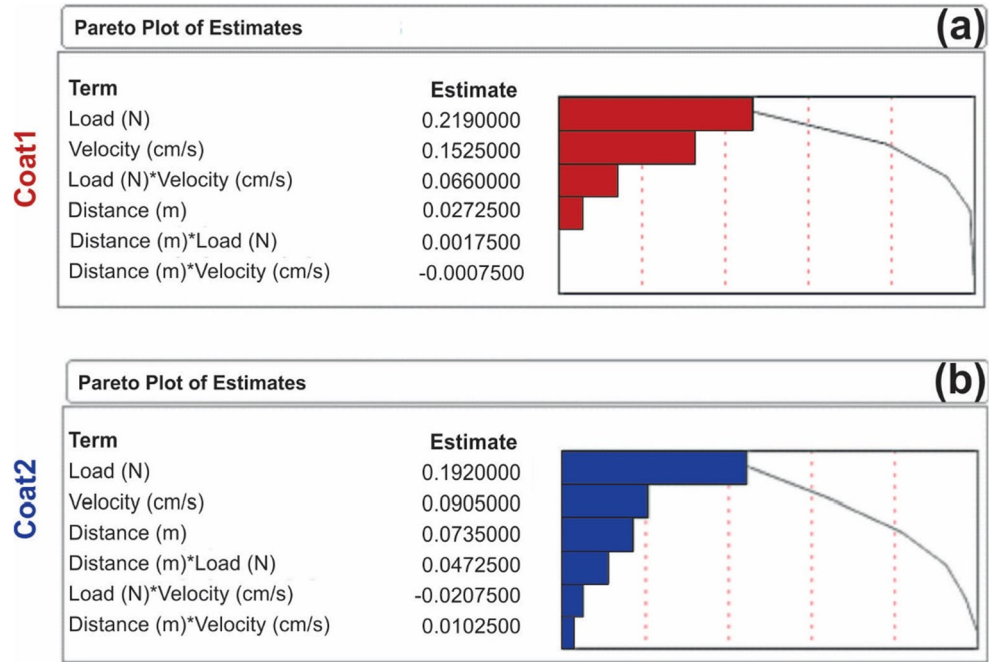


Fig. 10 Relation between experimental and predicted values of wear volume expressed in mm³ for both coatings. **a** Coat1 (NiCr-WC10Co4Cr) and **b** Coat2 (WC10Co4Cr)

Fig. 11 Pareto plot of estimates for wear test parameters on wear volume. **a** Coat1 (NiCr-WC10Co4Cr) and **b** Coat2 (WC10Co4Cr)



The experimental versus predicted values for both coatings are plotted in Fig. 10. It can be seen that the predicted values based on Eq. (2) are in good agreement with their corresponding experimental wear volume values of the input parameters (Fig. 10a). The square of the correlation coefficient values (R^2) and the square of the adjusted correlation coefficient

values (R^2_{adj}) for the model are, respectively, 0.999704 and 0.997931. R^2_{adj} value is close to 1.0, which means that the model (Eq. 2) has high reliability for predicting their corresponding experimental data. The general trend of Coat2 is found to be similar to previous published studies, which led to say that Coat2 has a good agreement with their

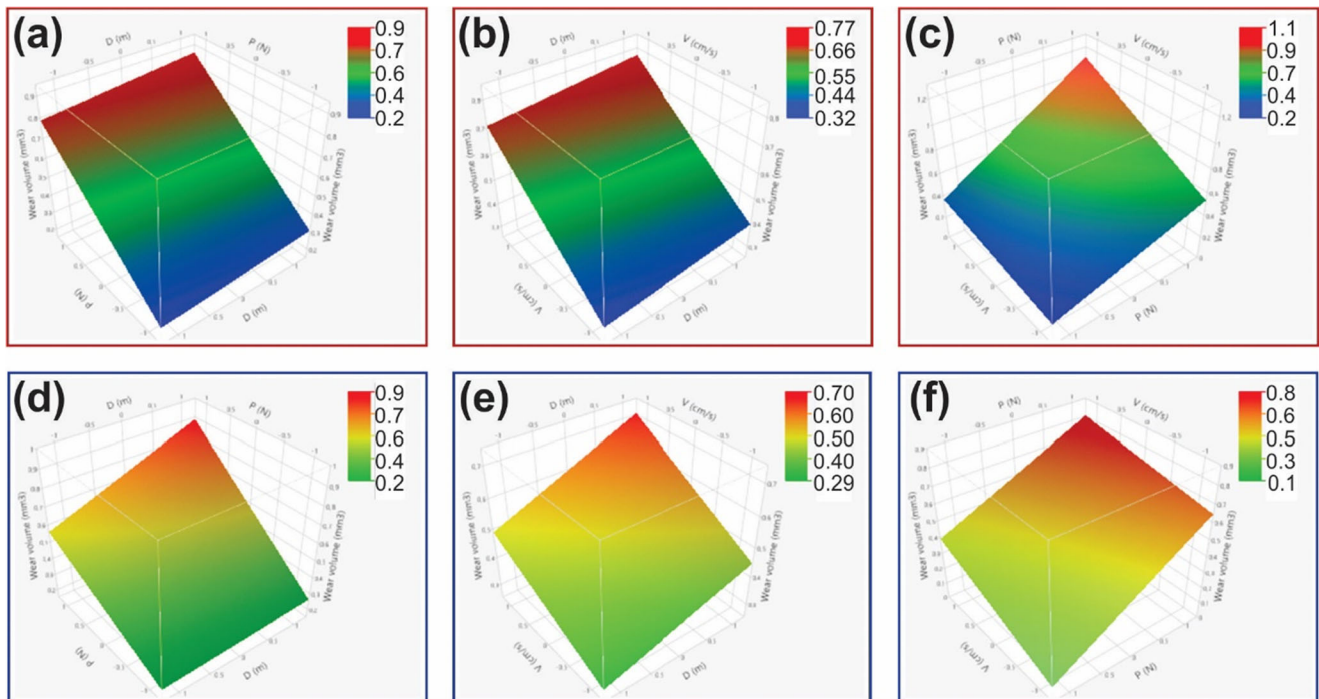


Fig. 12 Three-dimensional (3D) response surface interaction effect of factors on the wear volume of Coat1 (**a, b, c**) and Coat2 (**d, e, f**). **a** and **d** normal load (N)* sliding distance (m). **b** and **e** sliding velocity (cm/s)* sliding distance (m). **c** and **f** sliding velocity (cm/s)* normal load (N)

corresponding experimental wear volume value as clearly shown in Fig. 10b.

Figure 11 shows Pareto plot of estimates on the effect of wear test parameters for both coatings. It can be seen clearly that the single parameter with the highest effect on the wear volume is the normal load and then the velocity for the both coatings. However, the interaction between the load and the velocity is found to be in the third place for Coat1, while the distance is the one for Coat2. Note that the effect of wear parameters for the coatings could be different depending on the wear mechanism.

3D RSM interpretation curves of the regression equation are given in Fig. 12a, b, c, d, e, and f) to exhibit the relationship between the dependent variable, the experimental levels of each independent variable, and the interaction between two test variables when the third factor is kept at the middle level. For Coat1, the interaction effects between sliding distance-normal load (X_1, X_2) and sliding distance-velocity (X_1, X_3) on the wear volume are not significant with the increase of just

one parameter for each case. Moreover, the effect of the interaction between normal load and velocity (X_2, X_3) is the only significant interaction. The plot shows that the wear volume is increased with the increase of normal load and velocity. On the other hand, 3D response of surface plots for Coat2 shows the absence of interaction between sliding distance-sliding velocity and normal load-sliding velocity. Each parameter is impacting individually the variation of wear volume. Hence, the interaction between sliding distance-normal load is only the most significant parameter.

Figure 13 shows the prediction profiler function of the studied parameters. The optimum conditions wherein the best combination of factor settings for achieving the optimum response is found are at the minimum wear conditions (500m, 5N, and 5cm/s) for both coatings, with predicted response of 0.21775 mm^3 with a desirability value of 0.962 for Coat1 and 0.164 mm^3 with desirability value of 0.904 for Coat2.

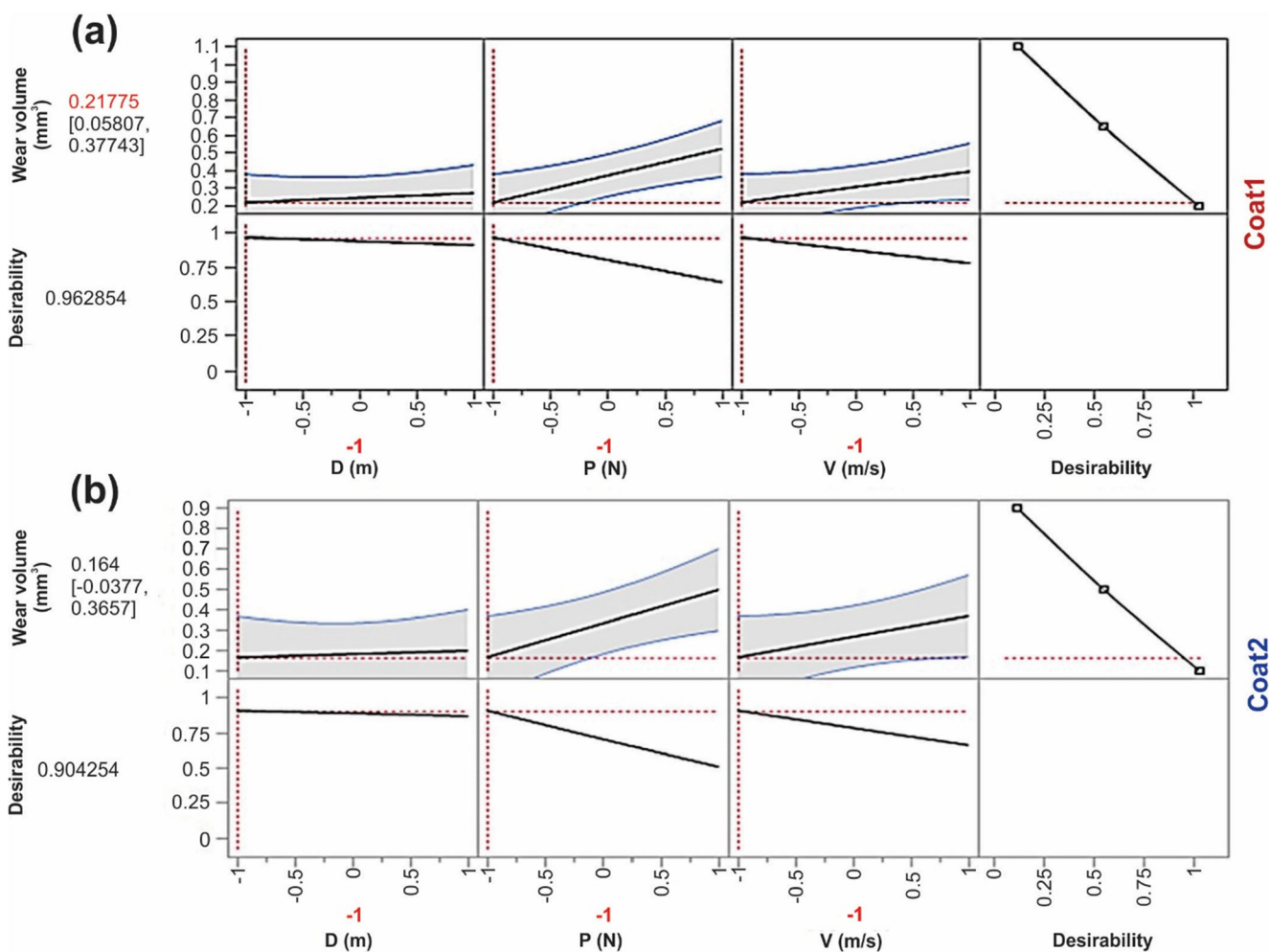


Fig. 13 Prediction profiler of wear volume (mm^3) function of parameters studied for both coatings. a Coat1 (NiCr-WC10Co4Cr) and b Coat2 (WC10Co4Cr)

4 Conclusions

In this study, the impact of wear test parameters (sliding distance, normal load, and sliding velocity) on the wear volume of NiCr-WC10Co4Cr (Coat1) and WC10Co4Cr (Coat2) HVOF coatings is investigated using microstructural analyses and RSM technique. The main conclusions obtained from this investigation can be summarized as follows:

- Microstructural properties of coating have a great influence in the wear behavior regarding to the presence of ductile or hard phase. Adhesive wear, with pull-out particle, and plastic deformation were observed on the surface of Coat1 due to the presence of NiCr ductile particles in the coating. On the other hand, abrasive wear mechanism is observed in Coat2 due to high hardness of WC10Co4Cr compared with that of NiCr matrix.
- Both coatings give the same response in terms of RSM when studying the impact of parameters individually, and the normal load is the most significant on wear volume. However, the combined wear test parameters impact on the wear behavior of coating differently with regard to their microstructure. 3D response surface interaction reveals that normal load-sliding velocity interaction is the most influencing in Coat1 while sliding distance-normal load interaction is the one in Coat2.

Acknowledgements The authors thank ETS Boudjellal metallizing for the preparation of the HVOF coatings and CRTI team for characterization help (Fabrication and Characterization Workshop).

Availability of data and material The authors confirm that the data supporting the findings of this study are available within the article. The raw data that support the findings of this study are available upon a reasonable request.

Code availability Not applicable (jmp 13 design of experiments “free version”)

Authors contribution Azzeddine Mazouzi: conceptualization, experimental work, data curation, and writing (original draft preparation). Amine Rezzoug: investigation, experimental work, reviewing, and editing. Billel Cheniti: methodology, reviewing and editing (final draft), review, and editing. Seif El Islam Lebouachera: software and analysis of all the obtained raw data of response surface methodology. Djamel Miroud: supervision and project administration. Aniss-Rabah Boukantar: validation. Nadjib Drouiche: methodology, validation, and involved in the discussion. Boubekeur Djerdjare: project administration.

Declarations

Ethics approval This study complies with the ethical standards set out by Springer. All the authors read and approved the final manuscript.

Conflict of interest The authors declare no competing interests.

References

1. Fauchais PL, Heberlein JV, Boulos MI (2014) Industrial applications of thermal spraying technology. In: Thermal spray fundamentals (pp 1401-1566). Springer, Boston, MA.
2. Davis JR (ed) (2004) Handbook of Thermal Spray Technology. TTS ASM Thermal Spray Society, ASM International, USA
3. Meng Y, Xu J, Jin Z, Prakash B, Hu Y (2020) A review of recent advances in tribology. *Friction* 8(2):221–300
4. Thakur L, Arora N (2013) Sliding and abrasive wear behavior of WC-CoCr coatings with different carbide sizes. *J Mater Eng Perform* 22(2):574–583
5. Dearnley PA, Aldrich-Smith G (2004) Corrosion–wear mechanisms of hard coated austenitic 316L stainless steels. *Wear* 256(5):491–499
6. Peat T, Galloway A, Toumpis A, Harvey D, Yang W-H (2016) Performance evaluation of HVOF deposited cermet coatings under dry and slurry erosion. *Surf Coat Technol* 300:118–127
7. Sidhu HS, Sidhu BS, Prakash S (2006) Mechanical and microstructural properties of HVOF sprayed WC-Co and Cr3C2-NiCr coatings on the boiler tube steels using LPG as the fuel gas. *J Mater Process Technol* 171(1):77–82
8. Fauchais PL, Heberlein JV, Boulos MI (2014) Thermal spray fundamentals: from powder to part. Springer Science & Business Media, NY, USA
9. Vicenzi J, Marques C, Bergmann C (2008) Hot and cold erosive wear of thermal sprayed NiCr-based coatings: influence of porosity and oxidation. *Surf Coat Technol* 202(15):3688–3697
10. Zhou W, Zhou K, Li Y, Deng C, Zeng K (2017) High temperature wear performance of HVOF-sprayed Cr3C2-WC-NiCoCrMo and Cr3C2-NiCr hardmetal coatings. *Appl Surf Sci* 416:33–44
11. Karaoglanli AC, Oge M, Doleker KM, Hotamis M (2017) Comparison of tribological properties of HVOF sprayed coatings with different composition. *Surf Coat Technol* 318:299–308
12. Azizpour MJ, Tolouei-Rad M (2019) The effect of spraying temperature on the corrosion and wear behavior of HVOF thermal sprayed WC-Co coatings. *Ceram Int* 45(11):13934–13941
13. Wickramarachchi CT, Rogers TJ, Leahy W, Cross EJ (2021) Predicting tool wear using linear response surface methodology and Gaussian process regression. *Topics in Modal Analysis & Testing*, vol 8. Springer, Boston, MA, pp 283–286
14. Kumar A, Kumar P, Singh B (2021) Optimizing the effect of wear test parameters on the specific wear rate of AZ91D magnesium alloy. *Mater Today: Proc*
15. Khuri AI, Mukhopadhyay S (2010) Response surface methodology. *Wiley Interdiscip Rev Comput Stat* 2(2):128–149
16. Huiping L, Guoqun Z, Shanting N, Yiguo L (2007) Technologic parameter optimization of gas quenching process using response surface method. *Comput Mater Sci* 38(4):561–570
17. Velmanirajan K, Thaheer ASA, Narayanasamy R, Basha CA (2012) Numerical modelling of aluminium sheets formability using response surface methodology. *Mater Des* 41:239–254
18. Saravanan I, Perumal AE, Vettivel S, Selvakumar N, Baradeswaran A (2015) Optimizing wear behavior of TiN coated SS 316L against Ti alloy using response surface methodology. *Mater Des* 67:469–482
19. Baradeswaran A, Vettivel S, Perumal AE, Selvakumar N, Issac RF (2014) Experimental investigation on mechanical behaviour, modelling and optimization of wear parameters of B4C and graphite reinforced aluminium hybrid composites. *Mater Des* 63:620–632
20. Sail K, Aouici H, Hassani S, Fnides B, Belaadi A, Naitbouda A, Abdi S (2017) Influence of tribological parameters on S335 steel filing Ti–W–N in dry sliding wear: prediction model and sliding

- condition optimization. *Int J Adv Manuf Technol* 92(9-12):4057–4071
21. Sharma S (2012) Wear study of Ni–WC composite coating modified with CeO₂. *Int J Adv Manuf Technol* 61(9-12):889–900
 22. Derringer G, Suich R (1980) Simultaneous optimization of several response variables. *J Qual Technol* 12(4):214–219
 23. Spliid H (2002) Design and analysis of experiments with k factors having p levels. Technical University of Denmark, Denmark
 24. Goupy J, Creighton L (2007) Introduction to design of experiments with JMP examples. SAS publishing
 25. Toma D, Brandl W, Marginean G (2001) Wear and corrosion behaviour of thermally sprayed cermet coatings. *Surf Coat Technol* 138(2-3):149–158
 26. Berger L-M, Saaro S, Naumann T, Wiener M, Weihnacht V, Thiele S, Suchánek J (2008) Microstructure and properties of HVOF-sprayed chromium alloyed WC–Co and WC–Ni coatings. *Surf Coat Technol* 202(18):4417–4421
 27. Murthy J, Bysakh S, Gopinath K, Venkataraman B (2007) Microstructure dependent erosion in Cr₃C₂–20 (NiCr) coating deposited by a detonation gun. *Surf Coat Technol* 202(1):1–12
 28. Xiang D, Cheng X-d, Xiang Y, Chao L, C-q Y, Z-x D (2018) Structure and cavitation erosion behavior of HVOF sprayed multi-dimensional WC–10Co4Cr coating. *Trans Nonferrous Metals Soc China* 28(3):487–494
 29. Mi P, Wang T, Ye F (2017) Influences of the compositions and mechanical properties of HVOF sprayed bimodal WC–Co coating on its high temperature wear performance. *Int J Refract Met Hard Mater* 69:158–163
 30. Mazouzi A, Djerdjare B, Triaa S, Rezzoug A, Cheniti B, Aouadi SM (2020) Effect of annealing temperature on the microstructure evolution, mechanical and wear behavior of NiCr–WC–Co HVOF-sprayed coatings. *J Mater Res* 35(20):2798–2807
 31. Oliver WC, Pharr GM (1992) An improved technique for determining hardness and elastic modulus using load and displacement sensing indentation experiments. *J Mater Res* 7(6):1564–1583
 32. Zhang Y, Epshteyn Y, Chromik RR (2018) Dry sliding wear behaviour of cold-sprayed Cu–MoS₂ and Cu–MoS₂–WC composite coatings: the influence of WC. *Tribol Int* 123:296–306
 33. Stott F, Wood G (1978) The influence of oxides on the friction and wear of alloys. *Tribol Int* 11(4):211–218
 34. Miguel J, Guilemany J, Vizcaino S (2003) Tribological study of NiCrBSi coating obtained by different processes. *Tribol Int* 36(3):181–187
 35. Cowan R, Winer W. *ASM Handbook: Vol. 18 Friction, Lubrication and Wear Technology*. ASM International, OH
 36. Cheniti B, Miroud D, Hvizdoš P, Balko J, Sedlák R, Csanádi T, Belkessa B, Fides M (2018) Investigation of WC decarburization effect on the microstructure and wear behavior of WC–Ni hardfacing under dry and alkaline wet conditions. *Mater Chem Phys* 208:237–247
 37. Mahmud TAB, Atieh AM, Khan TI (2017) The wear behavior of HVOF sprayed near-nanostructured WC–17% Ni (80/20) Cr coatings in dry and slurry wear conditions. *J Mater Eng Perform* 26(7):3507–3515
 38. Jarrah NA (2009) Studying the influence of process parameters on the catalytic carbon nanofibers formation using factorial design. *Chem Eng J* 151(1-3):367–371
 39. Gujarati DN (2004) *Econométrie, Traduction de la 4ième édition américaine par Bernard Bernier*. De Boeck, Bruxelles

Publisher's note Springer Nature remains neutral with regard to jurisdictional claims in published maps and institutional affiliations.